Accepted Manuscript

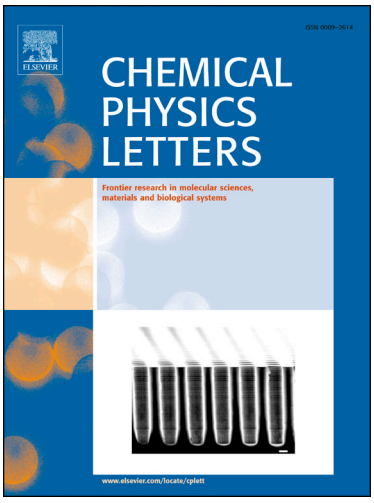

The effects of dielectric decrement and finite ion size on differential capacitance of electrolytically gated graphene

Lindsey Daniels, Matthew Scott, Z.L. Mišković

PII: S0009-2614(18)30315-4
DOI: https://doi.org/10.1016/j.cplett.2018.04.030
Reference: CPLETT 35586

To appear in: *Chemical Physics Letters*

Received Date: 21 January 2018
Accepted Date: 13 April 2018

Please cite this article as: L. Daniels, M. Scott, Z.L. Mišković, The effects of dielectric decrement and finite ion size on differential capacitance of electrolytically gated graphene, *Chemical Physics Letters* (2018), doi: https://doi.org/10.1016/j.cplett.2018.04.030

The effects of dielectric decrement and finite ion size on differential capacitance of electrolytically gated graphene

Lindsey Daniels[a], Matthew Scott[a], Z. L. Mišković[a,b,*]

[a] *Department of Applied Mathematics, University of Waterloo, Waterloo, Ontario, Canada N2L 3G1*
[b] *Waterloo Institute for Nanotechnology, University of Waterloo, Waterloo, Ontario, Canada N2L 3G1*

Abstract

We analyze the effects of dielectric decrement and finite ion size in an aqueous electrolyte on the capacitance of a graphene electrode, and make comparisons with the effects of dielectric saturation combined with finite ion size. We first derive conditions for the cross-over from a camel-shaped to a bell-shaped capacitance of the diffuse layer. We show next that the total capacitance is dominated by a V-shaped quantum capacitance of graphene at low potentials. A broad peak develops in the total capacitance at high potentials, which is sensitive to the ion size with dielectric saturation, but is stable with dielectric decrement.

Keywords: graphene, capacitance, electrolyte, dielectric decrement, steric effects

1. Introduction

Graphene has found many applications in electronics and photonics, but in recent years, a new application of graphene-based devices for biochemical sensing has materialized [1, 2, 3]. Typically, graphene-based sensors function as a field effect transistor (FET), where a single sheet of graphene acts as the conducting channel and is in contact with a liquid electrolyte [4]. Since graphene

*Corresponding author
Email address: zmiskovi@uwaterloo.ca (Z. L. Mišković)

is chemically inert and hydrophobic [5], the interface between graphene and the electrolyte is considered to be ideally polarizable, and therefore the insulating layer between the conducting channel and the electrolyte that typically arises in electrolyte-insulator-semiconductor FETs (EISFETs) can be eliminated [6]. Besides using graphene in a transistor mode, it was shown that operating graphene-based devices in the capacitor mode can provide additional advantages to sensing functionality [7]. When electrolytically gated, graphene's quantum capacitance has been shown to be much smaller than that of the electric double layer in the electrolyte [8, 9, 10], and as a consequence the surface potential on graphene exhibits more control over sensor output [11].

As a consequence of graphene's zero energy band gap, the electrical conductivity and differential capacitance of graphene-based FETs both exhibit minima as functions of the applied potential at the neutrality point, or point of zero charge [7, 11, 12]. This clear minimum, a unique feature of graphene, yields a more accurate sensing mechanism than previously seen, particularly in EISFETs, where shifts of the threshold potential are measured [6]. Experimental work has shown that graphene-based FETs are sensitive to changes in pH and/or ion concentration in the electrolyte, where typically either shifts in the capacitance or conductivity minimum of the device are observed [7, 13, 14]. It is known that graphene's π electron bands can yield a doping density in graphene of up to ~ 1 nm^{-2} [15]. This large doping density may give rise to strong electric fields (of up to ~ 13 V/nm) [15], which results in the *dielectric saturation* of solvent [16, 17, 18, 19, 20]. Large electric fields near graphene can also give rise to a prominent ion crowding, such that the effects of *finite ion size*, or steric effects become increasingly important [21, 22, 23, 24, 25].

We have recently studied in Refs. [26, 27] the effects of both finite ion size and dielectric saturation on the differential capacitance of electrolytically gated graphene by using the Bikerman-Freise (BF) model [28, 29] and the Booth model [30], respectively. However, large doping densities of graphene were found to be related to large potential drops across the electric double layer [26, 27]. This may give rise to significant *dielectric decrement* in the solvent, especially in

dense electrolytes, which is due to the excess polarizability of the hydrated ions [31, 32, 33, 34, 35, 36, 37]. Accordingly, our primary goal in this work is to explore the combined effects of finite ions size and dielectric decrement on differential capacitance of graphene over a large range of the potential applied through an aqueous ionic solution.

There was a large amount of work done to incorporate dielectric decrement into the framework of the Poisson-Boltzmann (PB) equation for an electrolyte with a metallic electrode [31, 32, 33, 34, 35, 36, 37], with some groups using a linearized decrement model to obtain analytical solutions to the modified PB (mPB) equation [32, 33, 34]. Since much of the experimental work for graphene in aqueous electrolytes uses ion concentrations below 2 M [7, 13, 14], we adopt here a linearized dielectric decrement model with empirical parameters [38], and combine it with the BF model for ion steric effects [28, 29]. This approach enables us to obtain an analytical expression for differential capacitance of the diffuse layer, and the total differential capacitance of graphene is obtained via a series connection of its quantum capacitance with that of the diffuse layer.

Our secondary goal in this work is to explore how combinations of the ion steric effect with dielectric saturation and dielectric decrement, treated separately, affect the dependence of the diffuse layer capacitance on the potential applied through that layer. Namely, it is well-known that the inclusion of ion steric effect in the mPB theory prevents excessive ion crowding at the interface between electrolyte and a metallic electrode, which causes the so-called "camel-shaped" or "M-shaped" capacitance of diffuse layer as a function of the potential [23]. Using the BF model gives rise to a change in the shape of that capacitance, going from a local minimum to a local maximum at the potential of zero charge (PZC) with increasing ion concentration. Finding a criterion that gives the ion concentration at which this cross-over from a "camel-shaped" to a "bell-shaped" capacitance takes place plays an important role in recent models of finite ion size effects in ionic liquids [23, 39, 40]. While we have found in our previous work how this criterion changes in the presence of dielectric saturation [27], we shall determine analogous criterion in this work in the presence of

dielectric decrement that generalizes the result found in Ref. [33].

After outlining the theoretical model, we discuss results for the diffuse layer capacitance and for the total capacitance of graphene, followed by our conclusions.

2. Theory

We start from a mean-field free-energy functional [25, 33, 34, 36], which will enable us to model the ion steric effects, dielectric saturation, and dielectric decrement in a self-consistent manner. After using the governing equations and the conditions for stationarity, we derive the diffuse layer capacitance from the first-integral. We then discuss the necessary modifications for a graphene electrode [26, 27]. Unless explicitly stated, we use Gaussian electrostatic units, where $4\pi\epsilon_0 \equiv 1$, with ϵ_0 being the dielectric permittivity of vacuum.

2.1. The Generalized Poisson-Boltzmann Equation

We consider a $z:z$ symmetric electrolyte, which contains positive and negative ions with concentration, $c_\pm$, and relative dielectric permittivity of solvent, ε. We start by minimizing the free energy, $F = U - TS$, of the system, where the electrostatic energy is

$$U = \int \Big[- w_e(\|\nabla\phi\|, c_+, c_-) + ze(c_+ - c_-)\phi - \mu_+ c_+ - \mu_- c_- \Big] d^3\vec{r}. \quad (1)$$

The first term is the self-energy of the electric field, which is given by [17]

$$w_e(\|\nabla\phi\|, c_+, c_-) = \frac{1}{4\pi} \int_0^{\|\nabla\phi\|} \varepsilon(E, c_+, c_-) E \, dE, \quad (2)$$

where we allow the dielectric permittivity to generally depend on the magnitude of the electric field, E, as well as on ion concentrations, $c_\pm$. Since no microscopic models are available for the full dependence of $\varepsilon(E, c_+, c_-)$ on all variables, one may resort to treating the dielectric saturation and dielectric decrement separately by allowing either $\varepsilon(E, c_+, c_-) = \varepsilon_{\rm sat}(E)$ or $\varepsilon(E, c_+, c_-) = \varepsilon_{\rm dec}(c_+, c_-)$,

respectively. In our previous work [27], we have studied the dielectric saturation by adopting the Booth model for $\varepsilon_{\rm sat}(E)$ [30] and proceeding to include the ion steric effects, as described below. In this work, we only present a derivation of the theory employing dielectric permittivity that describes dielectric decrement, which allows the integral in Eq. (2) to be evaluated as $w_e(\|\nabla\phi\|, c_+, c_-) = \varepsilon_{\rm dec}(c_+, c_-)\|\nabla\phi\|^2/(8\pi)$. The second term in Eq. (1) is the electrostatic energy of the ions in the potential ϕ, while the last two terms are the constraints for the conservation of the number of ions and are related to the chemical potentials of the bulk electrolyte, $\mu_\pm$.

The entropic portion of the free energy is derived from a lattice-gas model for cells of size a, which may be occupied by positive or negative ions, as well as water molecules [21, 22, 23]. For simplicity, we assume that the size of the ions and water molecules are the same and equal to a, and therefore, the entropic term is

$$-TS = \frac{k_BT}{a^3}\int \left[a^3c_-\ln(a^3c_-) + a^3c_+\ln(a^3c_+) + (1-a^3c_- - a^3c_+)\ln(1-a^3c_- - a^3c_+)\right] d^3\vec{r}, \tag{3}$$

with the negative and positive ions described by the first and second terms, respectively, and the water molecules by the last term. In the same manner, we assume that the excess polarizabilities of positive and negative ions are the same, $\alpha_+ = \alpha_- \equiv \alpha \geq 0$, so that the linearized model for dielectric decrement may be written as $\varepsilon_{\rm dec} = \varepsilon_w - \alpha(c_+ + c_-)$ [32, 33, 34, 36, 38], where ε_w is the dielectric constant of water (≈ 80). Then, minimizing the free energy with respect to ion concentrations yields

$$c_\pm = \frac{c_b e^{\mp ze\beta\phi} e^{-\frac{\alpha\beta}{8\pi}\|\nabla\phi\|^2}}{1-\nu+\nu e^{-\frac{\alpha\beta}{8\pi}\|\nabla\phi\|^2}\cosh(ze\beta\phi)}, \tag{4}$$

where $\beta = 1/(k_BT)$ is taken at room temperature, and $\nu = 2a^3c_b$ is the ion packing fraction from the steric effects, with c_b being the bulk concentration of both positive and negative ions. We note that the unmodified PB equation is returned by allowing $\nu \to 0$ and $\alpha \to 0$. The generalized PB equation in the

presence of dielectric decrement and steric effects is obtained by minimizing the free energy with respect to potential,

$$\nabla \cdot [\varepsilon_{\rm dec}(c_+, c_-)\nabla\phi] = -4\pi\rho, \tag{5}$$

where the volume charge density, $\rho = ze(c_+ - c_-)$, is expressed via Eq. (4). We note that if $\varepsilon_{\rm dec}$ is constant, i.e., $\alpha = 0$, then Eq. (5) is reduced to the mPB with ion steric effects described by the BF model [22, 23].

2.2. Diffuse Layer Capacitance

Solving the generalized PB equation in Eq. (5) in one dimension (1D) for the diffuse layer, which occupies the region $x \in [0, \infty)$, requires two boundary conditions for the potential $\phi(x)$, one at the interface with the electrode (graphene) at $x = 0$, $\phi(0) = \phi_0$, and the other in the bulk of the electrolyte, $\phi(x) \to 0$ and hence $\frac{d\phi}{dx} \to 0$ as $x \to \infty$. However, in order to obtain differential capacitance of the diffuse layer, it suffices to only find the first integral of Eq. (5). It is easier to obtain the first integral directly from the free energy $F = U - TS$ via the Beltrami identity, noting that the spatial variable x is missing in Eqs. (1) and (3). Denoting the electric field by $E = -\frac{d\phi}{dx}$, the first integral is

$$\frac{E^2}{8\pi}\left[\varepsilon_w - \frac{4\alpha c_b e^{-\frac{\alpha\beta}{8\pi}E^2}\cosh(ze\beta\phi)}{1-\nu+\nu e^{-\frac{\alpha\beta}{8\pi}E^2}\cosh(ze\beta\phi)}\right] - \frac{2c_b}{\beta\nu}\ln\Big[1-\nu+\nu e^{-\frac{\alpha\beta}{8\pi}E^2}\cosh(ze\beta\phi)\Big] = 0, \tag{6}$$

giving a relation between E and ϕ at any point $x \in [0, \infty)$, which expresses the condition of constant disjoint pressure in diffuse layer [25].

The differential capacitance of diffuse layer per unit area is defined as $C_d = \frac{d\sigma_d}{dV_d}$, where σ_d is the total charge density per unit area in diffuse layer and $V_d = -\phi_0$ is the potential drop across that layer [27]. Bazant *et al.* [24] showed that the diffuse layer capacitance may be generally expressed as $C_d = -\rho_0/E_0$, where E_0 is the value of the electric field E at $x = 0$, and $\rho_0 = ze\left(c_+^0 - c_-^0\right)$ is the volume charge density in the electrolyte evaluated at $x = 0$, with $c_\pm^0$ being given by Eq. (4) upon replacements $\|\nabla\phi\| \to |E_0|$ and $\phi \to \phi_0$. Thus, one could

solve Eq. (6) numerically for E_0 in terms of ϕ_0 and use Eq. (4) at $x = 0$ to evaluate the diffuse layer capacitance C_d for any given value of the potential, $\phi_0 = -V_d$. To that effect, it is convenient to introduce dimensionless parameters $\tilde{\alpha} = \alpha c_b/\varepsilon_w$ and $\tilde{E} = E_0/E_c$, where $E_c = \sqrt{8\pi c_b/(\beta\varepsilon_w)}$. Then, from Eq. (4), the diffuse layer capacitance may be written as

$$C_d = \frac{C_D}{\tilde{E}} \frac{e^{-\tilde{\alpha}\tilde{E}^2} \sinh(ze\beta V_d)}{1 - \nu + \nu e^{-\tilde{\alpha}\tilde{E}^2} \cosh(ze\beta V_d)}, \tag{7}$$

where $C_D = \varepsilon_w/(4\pi\lambda_D)$ is the Debye capacitance, with $\lambda_D^{-1} = \sqrt{8\pi\beta z^2 e^2 c_b/\varepsilon_w}$ being the inverse Debye length of the electrolyte.

However, it is interesting that Eq. (6) may be solved explicitly for the potential $\phi_0 = -V_d$ in terms of E_0. Using the dimensionless parameters $\tilde{\alpha}$ and $\tilde{E}$, we obtain from Eq. (6)

$$V_d = \frac{1}{ze\beta} \operatorname{arccosh}\left(\frac{1-\nu}{\nu} \mathrm{e}^{\tilde{\alpha}\tilde{E}^2}\left[-1 + \frac{2\tilde{\alpha}\tilde{E}^2}{\mathcal{L}(\tilde{E})}\right]\right), \tag{8}$$

where $\mathcal{L}(\tilde{E}) = \mathrm{W}\left(2\tilde{\alpha}\tilde{E}^2(1-\nu)\mathrm{e}^{\left(2\tilde{\alpha}-\frac{\nu}{2}\right)\tilde{E}^2}\right)$, with W being the Lambert-W function. By substituting V_d from Eq. (8) into right-hand side of Eq. (7) one obtains C_d as a function of $\tilde{E}$. Thus, an analytical relation between the diffuse layer capacitance and the diffuse layer potential drop is obtained by considering the obtained $C_d(\tilde{E})$ and $V_d(\tilde{E})$ from Eq. (8) as parametric functions with the normalized electric field, $\tilde{E} = E_0/E_c$, being the parameter. Such relation is useful, e.g., in analyzing the cross-over from a "camel-shaped" to a "bell-shaped" capacitance C_d as a function of the potential when $V_d \to 0$.

Moreover, by applying Gauss' law to the diffuse layer, we may write $\sigma_d = -\varepsilon_0 E_0/(4\pi)$, where $\varepsilon_0 \equiv \varepsilon_w - \alpha\left(c_+^0 + c_-^0\right)$ is the value of the dielectric permittivity $\varepsilon_{\mathrm{dec}}$ at $x = 0$. With $c_\pm^0$ being given by Eq. (4) at $x = 0$, we may substitute $\phi_0 = -V_d$ from Eq. (8) into that equation and use the Gauss' law to express the charge density per unit area in the diffuse layer as a function of the normalized electric field, $\sigma_d(\tilde{E})$. This enables us to make contact with the charge density on graphene.

2.3. Including Quantum Capacitance of Graphene

In our previous work [26, 27], we showed quite generally how to include a graphene electrode into this framework. Allowing for a charge-free Stern (or compact) layer with capacitance C_S, which is positioned between the diffuse layer and graphene, the total differential capacitance of electrolytically gated graphene may be expressed as a series connection of three capacitors, $C_{\rm tot} = \left(C_d^{-1} + C_S^{-1} + C_g^{-1}\right)^{-1}$, with C_g being the quantum capacitance of single-layer graphene (SLG), see, e.g., Ref. [27]. Unlike metallic electrodes, graphene exhibits strong effects due to smallness of its quantum capacitance near the PZC, which is a consequence of the low-energy properties of the electronic band structure in carbon based materials.

Historically, the first accounts of the role of electronic capacitance of carbon electrodes in electrolyte were given in classical papers by Yeager and Gerischer [41, 42], followed by the first theoretical interpretation [43] and a decisive experimental confirmation of the effect, published much later [44]. All those studies reported V-shaped capacitances with a rounded minimum that attains a surprisingly low value, on the order of 1 μF/cm^{-2} at the PZC. The first combination of the electronic capacitance of a graphite electrode and the double layer in ionic liquids was given recently by Kornyshev *et al.* [45]

On the other hand, there is insufficient information at this time about the Stern layer capacitance of the graphene-solvent interface, C_S, partly because the total capacitance, $C_{\rm tot}$, is completely dominated by the smallness of the quantum capacitance of graphene near the PZC. While it would be possible to use the above expression for $C_{\rm tot}$ by treating C_S phenomenologically, as was done in Ref. [27], we remark that precise modeling of C_S at the graphene-solvent interface would require a more subtle analysis [13, 46, 47, 48], which lies beyond the scope of the present work. Nevertheless, we expect that useful information on the qualitative behavior of the total differential capacitance for electrolytically gated graphene may be obtained by ignoring the role of the Stern layer, so we proceed by studying a series connection of the capacitance of the diffuse layer, C_d, and the quantum capacitance of graphene, C_g.

As in Refs. [26, 27], we use the definition $C_g = -\frac{d\sigma_g}{dV_g}$, where σ_g is the surface charge density on graphene and $V_g = \mathcal{E}_F/e$ is its doping potential, with $\mathcal{E}_F$ being the Fermi energy in graphene relative to its Dirac point. For charge carrier densities in graphene up to ~ 1 nm^{-2}, which are typically achieved for doping potentials up to $|V_g| \sim 1$ V, one may use the Dirac cone approximation for graphene's π electron bands, giving [26]

$$\sigma_g = \frac{2}{\pi}\frac{e}{\left(\hbar v_{\mathrm{F}}\beta\right)^2}\left[\mathrm{dilog}\left(1+\mathrm{e}^{\beta e V_g}\right) - \mathrm{dilog}\left(1+\mathrm{e}^{-\beta e V_g}\right)\right], \tag{9}$$

where dilog is the standard dilogarithm function, and $v_F \approx 10^6$ m/s is the Fermi speed in graphene. As a result, we obtain

$$C_g = \frac{4e^2}{\pi\beta\left(\hbar v_{\mathrm{F}}\right)^2}\ln\left[2\cosh\left(\beta e V_g/2\right)\right], \tag{10}$$

which attains a minimum value of $\approx 0.8\ \mu$F/cm^2 for $V_g = 0$ at room temperature and exhibits a linear increase with the potential according to $C_g \propto |V_g|$ for $\beta e|V_g| \gtrsim 1$, as a signature of the Dirac cone approximation.

Defining the total applied potential as $V_a = V_d + V_g$, we obtain the total differential capacitance of electrolytically doped graphene as

$$C_{dg} = \frac{C_d\, C_g}{C_d + C_g}, \tag{11}$$

where a relation between V_d and V_g is determined via the charge neutrality of the system, $\sigma_g + \sigma_d = 0$ [27]. It is worthwhile mentioning that this condition enables us to express the charge density on graphene as $\sigma_g(\tilde{E}) = -\sigma_d(\tilde{E})$, where $\tilde{E} = E_0/E_c$ is the normalized electric field at the graphene/electrolyte interface. By expressing V_g in terms of σ_g via Eq. (9), one can ultimately obtain both V_g and C_g from Eq. (10) as functions of $\tilde{E}$. Therefore, $\tilde{E}$ is a common parameter, shared by the quantities that pertain to both the diffuse layer and the quantum capacitance, enabling one to study, e.g., the relation between the total capacitance in Eq. (11) and the total applied potential by treating them as parametric functions, $C_{dg}(\tilde{E})$ and $V_a(\tilde{E})$.

Moreover, we can use a parametric representation for $V_d(\tilde{E})$ from Eq. (8) and the above obtained function $V_g(\tilde{E})$ to analyze the split of a given total applied

potential, V_a, into the potential drop across the diffuse layer and the doping potential of graphene. In this way, we can avoid a numerical solution of a complicated system of equations for E_0 and $\phi_0 = -V_d$, which would involve Eq. (6) at $x = 0$ and the neutrality condition written in the form $\sigma_g = \varepsilon_0 E_0/(4\pi)$, where σ_g is given by Eq. (9) with $V_g = V_a - V_d$.

3. Results and Discussion

We first analyze the differential capacitance of the diffuse layer, C_d, as a function of the potential drop across that layer, V_d, taking into account steric effects given by the BF model and dielectric decrement, as discussed in the previous section. We also make comparisons with results from our previous work [27], where we analyzed steric effects given by the BF model and dielectric saturation effects given by the Booth model. Since C_d is even function of V_d under the model assumptions adopted here, we only show results for $V_d \geq 0$. Referring to the data used in Refs. [32, 33], we use $\alpha = 3$ M^{-1} and $\alpha = 12$ M^{-1} as lower and upper bounds for typical values of the coefficients in the linearized dielectric decrement model. As for the steric effect, we use in most calculations Bjerrum length at room temperature, $a \approx 0.71$ nm, as an upper bound for typical ion sizes [27, 32, 33].

We discuss several model combinations, which we label appropriately for the ease of comparison. Considering various effects separately, we label the steric effect by S, dielectric decrement by D, and dielectric saturation treated via the Booth model by B. A combination of the steric effect with the dielectric decrement is labeled by D+S, whereas combination of the steric effect with the dielectric saturation via the Booth model is labeled by B+S. The model involving point ions with constant dielectric permittivity of solvent is naturally referred to as the PB model.

3.1. Diffuse Layer Capacitance

In the panels (a) and (b) of Fig. 1, we see that the U-shaped capacitance of the simple PB model is changed to a "camel-shaped" form (at low ion con-

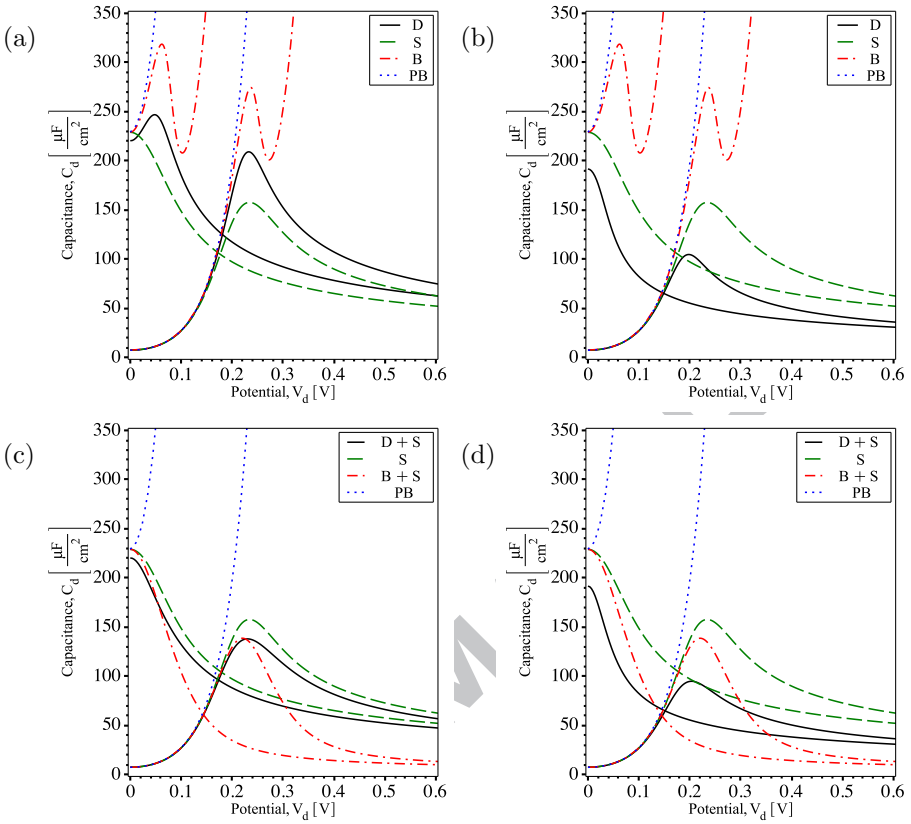

Figure 1: Panels (a) and (b) show comparisons of the diffuse layer capacitance C_d for the cases when only the steric effect (S), dielectric decrement (D), or dielectric saturation via Booth model (B) is taken into account, as well as for the simple Poisson-Boltzmann (PB) case. Panels (c) and (d) show comparisons of C_d for a combination of the steric effect with dielectric decrement (D+S) and a combination of the steric effect with dielectric saturation via the Booth model (B+S), along with the case when only the steric effect (S) is taken into account and with the simple PB case. Results are shown for the bulk ion concentrations $c = 1$ M and $c = 10^{-3}$ M (curves shifted to the right). In the panels (a) and (c) we use $\alpha = 3$ M^{-1}, while in the panels (b) and (d) we use $\alpha = 12$ M^{-1}. In all cases the steric effect is treated via the BF model with $a = 0.71$ nm.

centrations c) or "bell-shaped" form (for sufficiently large ion concentrations c) due to either the S model or D model, whereas the B model only gives an offset to the U-shape in the form of a closely-spaced local peak-and-valley pair. While the large V_d behavior of the capacitance C_d follows the inverse square-root

asymptotics deduced before for the S model [23, 24, 27] and for the D model [32, 33], C_d is seen to continue to increase without bound with increasing V_d for the B model in a manner that parallels the increase in the PB model.

In the panels (c) and (d) of Fig. 1, we demonstrate the effects of combining the D and S models (D+S) or B and S models (B+S). One notices that, for the smaller value of ion polarizability, $\alpha = 3$ M^{-1}, used in the panels (a) and (c), there is a relatively strong interplay of the steric and dielectric decrement effects, such that, e.g., a "camel-shaped" capacitance with shallow minimum at $V_d = 0$, seen in the panel (a) for the D model with ion concentration of $c = 1$ M, becomes "bell-shaped" in the panel (c) for the D+S model with the same ion concentration. On the other hand, for the larger value of $\alpha = 12$ M^{-1}, used in the panels (b) and (d), one sees very little differences between the models D and D+S, showing that the dielectric decrement prevails over the steric effect, even for a relatively large ion size of $a = 0.71$ nm. At the same time, the B+S model exhibits quite dramatic effect on the capacitance for the potential values beyond the peak positions, which is observed as a significant lowering of C_d for large V_d values for the B+S model in the panels (c) and (d), when compared to the corresponding curves for the S model in the panes (a) and (b). This reduction of C_d by a factor $n/\sqrt{\varepsilon_w}$, where $n \approx 1.33$ is the optical refractive index of water, is a somewhat unexpected consequence of a strong interplay of dielectric saturation and steric effects in the B+S model for asymptotically large V_d, which was analyzed in detail in Ref. [27].

In Fig. 2, we explore a range of small values of the potential V_d for the capacitance C_d obtained by using the D+S and B+S combinations of models. We display a range of ion concentrations c that exhibits cross-over from a "camel-shaped" to a "bell-shaped" capacitance for both models with increasing c values. We recall that in the S model, i.e., in the absence of dielectric saturation and dielectric decrement effects, a condition for this cross-over is $\nu \equiv 2a^3c > 1/3$, as deduced by Kornyshev *et al.* [23, 40, 49] from the BF model for ion steric effects in ionic liquids. With $a = 0.71$ nm, this occurs for ion concentrations $c > 0.77$ M in the bulk electrolyte. For the B+S model, we have derived in Ref. [27] a

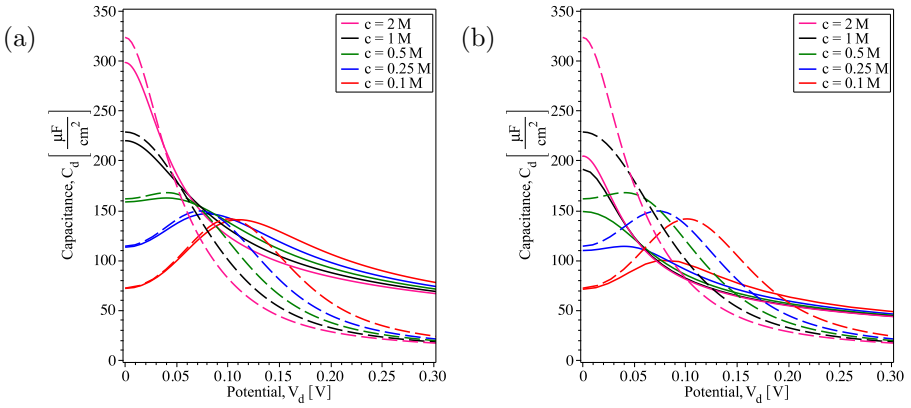

Figure 2: A comparison of the diffuse layer capacitance C_d for a model combining the dielectric decrement with ion steric effects (solid lines), and a model combining the dielectric saturation via the Booth model with ion steric effects (dashed lines), for the bulk ion concentrations between $c = 0.1$ M and $c = 2$ M. While for all curves the ion size is $a = 0.71$ nm, the ion polarizability coefficient takes values $\alpha = 3$ M^{-1} (panel a) and $\alpha = 12$ M^{-1} (panel b).

generalization of that condition as

$$3\nu - 1 + \left(\varepsilon_w - n^2\right)\frac{16\pi c}{5\beta E_{\rm sat}^2} > 0, \tag{12}$$

where $E_{\rm sat} \sim 1$ V/nm is a critical electric field for which the dielectric saturation sets in within the Booth model [30]. With the same ion size, one obtains a somewhat reduced critical value of ion concentration for the cross-over, $c > 0.66$ M.

Using the parametric representation of the relation between C_d and V_d from the previous section, we obtain a new generalization of the condition for the "camel-to-bell" shape cross-over of the diffuse layer capacitance at $V_d = 0$ for the D+S model as

$$48\nu\tilde{\alpha}^2 - 40\tilde{\alpha}^2 - 24\nu\tilde{\alpha} + 16\tilde{\alpha} + 3\nu - 1 > 0, \tag{13}$$

where $\tilde{\alpha} \equiv \alpha c/\varepsilon_w$. Again using the ion size $a = 0.71$ nm, we find the critical ion concentrations for the cross-over to be $c > 0.61$ M for $\alpha = 3$ M^{-1} and $c > 0.34$ M for $\alpha = 12$ M^{-1}. These values are corroborated by the shape of the curves shown in Fig. 2 in the limit $V_d \to 0$.

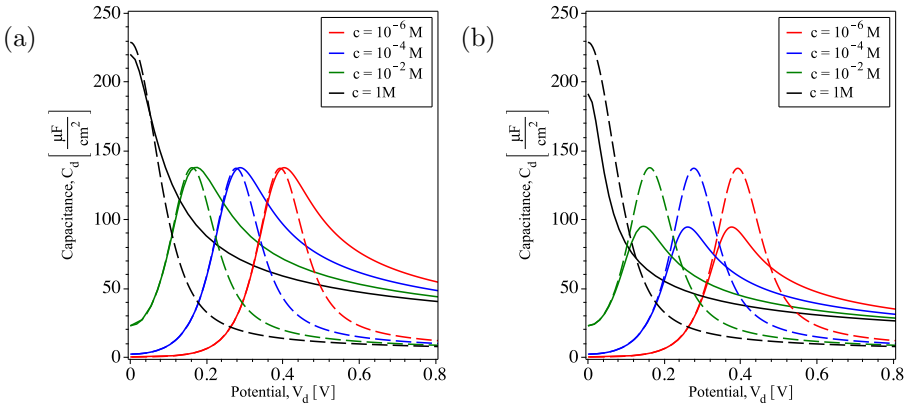

Figure 3: A comparison of the diffuse layer capacitance C_d for a model combining the dielectric decrement with ion steric effects (solid lines), and a model combining the dielectric saturation via the Booth model with ion steric effects (dashed lines), for ion concentrations $c = 10^{-6}$ M, $c = 10^{-4}$ M, $c = 10^{-2}$ M and $c = 1$ M. While for all curves the ion size is $a = 0.71$ nm, the ion polarizability coefficient takes values $\alpha = 3$ M^{-1} (panel a) and $\alpha = 12$ M^{-1} (panel b).

In Fig. 3, we focus on the behavior of the peaks in the "camel-shaped" capacitance C_d for the D+S and B+S models at very low ion concentrations in the bulk electrolyte, $c \ll 1$ M (we only show the case $c = 1$ M for reference). As anticipated in the panels (c) and (d) of Fig.1, one can see in Fig. 3 that the two models give almost identical capacitance curves for small potentials, which arise from the prevalence of the PB model at low ion concentrations and small potentials. For $\alpha = 3$ M^{-1}, the peak positions and peak heights happen to be almost identical for the two models, whereas for $\alpha = 12$ M^{-1} the peaks' positions are lower and their heights are significantly smaller in the D+S model with respect to those in the B+S model. Interestingly, the peak heights in both models are independent of ion concentrations, while the peak positions seem to increase in proportion to $\ln c$ for $c \ll 1$ M. Those observations can be rationalized by considering the asymptotic behavior of C_d for large V_d, found for the S model in Refs. [23, 24, 27] and for the D model in Refs. [32, 33]. Namely, both models yield a generic asymptotic form $C_d^{(\mathrm{as})} \sim 1/\sqrt{X}$, which captures the dependence on both the potential V_d *and* ion concentration c with

$X = \beta z e V_d + \ln(\nu/2)$ for the S model and $X = \beta z e V_d + \ln(2\tilde{\alpha})$ for the D model. An estimate for the peak positions in the "camel-shaped" curves in Fig. 3 can be then obtained by equating $C_d^{(\mathrm{as})}$ with the diffuse layer capacitance in the PB model, C_{PB}. Remarkably, the dependence of C_{PB} on the potential *and* ion concentration may be expressed compactly for large potentials in terms of the above variable X as $C_{PB}^{(\mathrm{as})} \sim \mathrm{e}^{X/2}$. Then, solving the equation $C_{PB}^{(\mathrm{as})} = C_d^{(\mathrm{as})}$ yields the X values that reproduce qualitative features of the curves for both models in Fig. 3 for $c \ll 1$ M.

It should be stressed that values of the diffuse layer capacitance shown in Figs. 1-3 are unrealistically high in comparison to the values measured in aqueous solutions with metallic electrodes at ionic concentrations $c \sim 1$ M, see, e.g., [24, 32, 46]. This is a consequence of our using a continuous description of the solvent dielectric response described in terms of the local dielectric constant, dependent on ion concentrations and electric field. Namely, the effects of molecular structure of the solvent are very important at the nanoscale distances from an electrode [15]. These effects can be incorporated within a mean field approach by invoking a compact layer (interchangeably called inner layer, or Helmholtz layer, or Stern layer), giving rise to the so-called Gouy-Chapman-Stern-Grahame model, discussed in detail in Ref. [46]. As a result, the total capacitance of a double layer formed at the interface with a metallic electrode can be represented as a series connection of the diffuse layer capacitance, C_d, and the Stern layer capacitance, C_S. The properties of such compact layer can be deduced from a microscopic picture of the metal-electrolyte interface within a nonlocal dielectric formalism [47, 48], giving values on the order of $C_S \sim 10$ $\mu\mathrm{F/cm}^{-2}$ [46].

Alternatively, a Stern layer capacitance may be simply treated as an empirical parameter, as in Refs. [24, 32, 37], where a correct order of magnitude matching the experimental data was achieved using the values $C_S = 125$, 146, and ≈ 155 $\mu\mathrm{F/cm}^{-2}$, respectively. The main effect of the Stern layer capacitance is to reduce the value of the total double layer capacitance near the PZC for high ion concentrations, as well as at high potential values, where the effects

of finite ion size and/or dielectric decrement give rise to peaks in a "camel-shaped" capacitance. It is interesting that such smoothening of the capacitance curves, and reduction of the absolute values at their extrema, may be achieved by introducing short-range correlations between ions in the lattice gas model, thereby bypassing the necessity to introduce a Stern layer into the theory [40].

3.2. Including Quantum Capacitance of Graphene

Regarding the Stern layer capacitance of a graphene-solvent interface, far less is known than in the case of metallic electrodes. For example, recent measurements of the capacitance of carbon based electrical double layer capacitors in a 6M KOH aqueous electrolyte showed that, unlike the case of multi-layer graphene, the inferred Stern layer capacitance for a SLG electrode changes quite rapidly, and in a rather asymmetric manner, taking values in the range from $C_S \approx 17$ μF/cm^{-2} up to ≈ 60 μF/cm^{-2} when the potential drop across that layer deviates by some 0.05 V from the PZC (see Fig. 4(d) in Ref. [13]). In our previous work, we have deduced a value of $C_S \approx 60$ μF/cm^{-2} for the B+S model combination by adopting a simple model for the Stern layer placed next to graphene, which is consistent with the lattice gas model for ion steric effects and with the dielectric saturation in solvent. Namely, we have evaluated C_S for a layer of water of thickness $a/2$ with uniform dielectric permittivity determined from $\sigma_g = \varepsilon_{\rm sat}(E_0)E_0/(4\pi)$, which clearly depends on the charge density on graphene σ_g, but not on the ion concentration in the electrolyte [27]. It would be difficult to adapt such model of Stern layer in a consistent manner to the D+S model combination, since dielectric decrement depends on ion concentration in the electrolyte. Therefore, given the uncertainty regarding proper modeling of the Stern layer for SLG in general, and aiming at a comparison of the effects of the D+S and B+S model combinations on electrolytically gated graphene in particular, we only consider here a series connection of the capacitance of the diffuse layer, C_d, and the quantum capacitance of graphene, C_g, given in Eq. (11).

In Fig. 4(a) we show the dependence of C_{dg}, given in Eq. (11), on the total

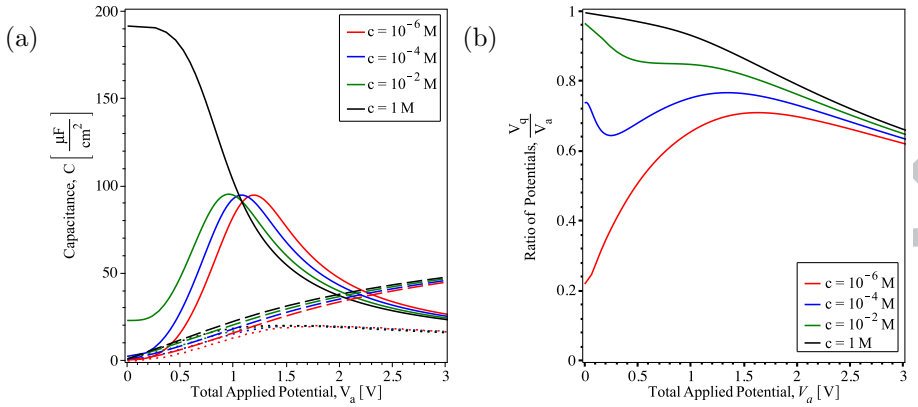

Figure 4: The diffuse layer capacitance C_d (solid lines), the quantum capacitance C_g (dashed lines), and the total capacitance C_{dg} from Eq. (11) (dotted lines) are shown in panel (a) as functions of the total applied potential $V_a = V_d + V_g$ for a model of C_d that combines the dielectric decrement with ion steric effects for ion concentrations $c = 10^{-6}$ M, $c = 10^{-4}$ M, $c = 10^{-2}$ M and $c = 1$ M, with fixed ion size $a = 0.71$ nm, and the ion polarizability coefficient $\alpha = 12$ M^{-1}. The corresponding values of the ratio of the doping potential in graphene, V_g, to the total applied potential V_a are shown in panel (b).

applied potential $V_a = V_d + V_g$ in a broad range of ion concentrations. We only consider in Fig. 4 the case where C_d is calculated with the model labeled D+S, which combines the dielectric decrement with steric effects, using the same parameters as those corresponding to the solid curves in Fig. 3(b). Besides the results for C_{dg}, we also show in Fig. 4(a) separate results for C_d and C_g as functions of V_a, each evaluated with the corresponding values of the potential components, V_d and V_g, respectively. One notices in Fig. 4(a) that the quantum capacitance C_g of graphene is very small at the applied potentials $V_a \lesssim 1$ V and, hence, it dominates in C_{dg} at such potentials for all ion concentrations, except the lowest one, $c = 10^{-6}$ M. Accordingly, the strong dependence of C_d on the ion concentration at low potentials is suppressed in C_{dg}. On the other hand, as the applied potential increases, say for $V_a \gtrsim 1$ V, C_d starts exhibiting the $C_d \propto 1/\sqrt{|V_d|}$ dependence, whereas C_g continues to increase, so that a broad peak develops in C_{dg} in the range $1.5 \lesssim V_a \lesssim 2$ V in Fig. 4(a). We note that such peak could be manifested in experiments as saturation of the total

capacitance with increasing applied potential.

In Fig. 4(b), we show the ratio V_g/V_a of the doping potential of graphene to the total applied potential V_a as a function of that potential. One notices that, owing to the smallness of C_g with respect to C_d, generally a quite large fraction of the applied potential goes to doping the graphene, except for small applied potentials, $V_a \lesssim 1$ V, at the lowest ion concentration, $c = 10^{-6}$ M. For example, one observes in Fig. 4(b) that, at the potential $V_a \approx 1.6$ V, where C_{dg} exhibits a broad maximum for ion concentrations $10^{-4} < c < 10^{-2}$ M in Fig. 4(a), the doping potential of graphene is quite large, $V_g \approx 1.3$ V, whereas the value of $V_d \approx 0.3$ V confirms the prevalence of the $C_d \propto 1/\sqrt{|V_d|}$ dependence of the diffuse layer capacitance seen in Fig. 3(b).

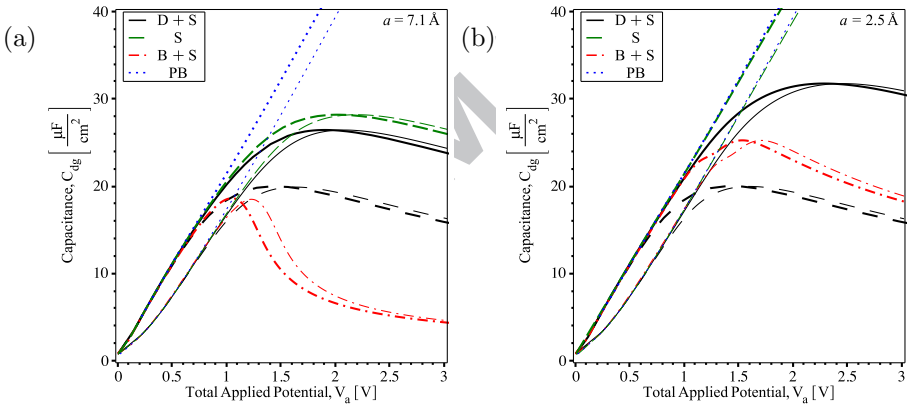

Figure 5: A comparison of total capacitance C_{dg} with the diffuse layer capacitance obtained with different models: a combination of dielectric decrement with ion steric effects (D+S, black lines), a combination of dielectric saturation via the Booth model with ion steric effects (B+S, red dash-dotted dashed lines), a model with ion steric effects alone (S, green dashed lines), and the simple Poisson-Boltzmann model (PB, blue dotted lines). All results are shown for ion concentrations $c = 10^{-3}$ M (thin lines) and $c = 1$ M (thick lines). The D+S model is shown for ion polarizability coefficients $\alpha = 3$ M^{-1} (solid black lines) and $\alpha = 12$ M^{-1} (dashed black lines). The ion size in the models involving steric effects is taken to be $a = 0.71$ nm (panel a) and $a = 0.25$ nm (panel b).

Finally, in Fig. 5 we discuss the total differential capacitance, C_{dg}, given in Eq. (11), for a low and a high ion concentration and two ion sizes. We compare

the cases when C_d is obtained with the simple PB model, S model, and the combinations D+S and B+S. The most striking effect seen in the figure is that all the cases are almost identical for the applied potentials $V_a \lesssim 1$ V, owing to the fact that quantum capacitance C_g of graphene is very small at such potentials. As in Fig. 4(a), one notices that there is a relatively small change in the shape of C_{dg} when ion concentration changes from $c = 1$ M to $c = 10^{-3}$ M. For both concentrations, the quasi-linear dependence of C_{dg} on V_a comes from the characteristic V-shaped dependence of the quantum capacitance C_g of graphene on its doping potential V_g.

While C_g continues to dominate when combined with C_d obtained with the PB model, giving its linear dependence for larger V_a values in Fig. 5, one notices that, when the model combinations D+S and B+S are used for C_d, there arises a maximum in C_{dg} for $V_a \gtrsim 1$ V. This maximum is strongly dependent on the ion size, except in the case of the D+S model with large ion polarizability coefficient of $\alpha = 12$ M^{-1}, which was studied in Fig. 4. One sees that the rather narrow peak near $V_a = 1$ V for the B+S model with $a = 0.71$ nm in Fig. 5(a) becomes broader and taller, and it moves to $V_a \sim 1.5$ V, when the ion size is reduced to $a = 0.25$ nm for the B+S model in Fig. 5(b). A structure seen in the region $1 \lesssim V_a \lesssim 1.5$ V for the curves labeled B+S in Fig. 5(b) is a signature of the competition between the ion steric effects and dielectric saturation, discussed at length in Ref. [27].

Probably the most dramatic effect of reducing the ion size is observed for the curves labeled S, when C_d is only modeled by including the ion steric effects via the BF model. One sees that the broad peak at $V_a \sim 2$ V in the curves labeled S in Fig. 5(a) completely disappears for the smaller ion size in Fig. 5(b). Moreover, the curves labeled S in that figure practically coincide with the curves labeled PB for point ions ($a = 0$). This echoes the observation made by Bazant *et al.* [24] in studying the BF model, where unreasonably large ion sizes had to be used to give rise to "camel-shaped" capacitance for metallic electrodes in aqueous solutions. At the same time, the curves labeled D+S in Fig. 5(b) still exhibit a broad peak for electrolytically gated graphene at the potential values

$2 \lesssim V_a \lesssim 2.5$ V, which persists even in the limit of point ions. Hence, given that there is some uncertainty regarding the appropriate choice for ion sizes [24], it seems that only a combination of the ion steric effects with dielectric decrement is capable of giving rise to a stable, broad peak in the total capacitance C_{dg} at the applied potentials $V_a \gtrsim 1$ V. While a conclusive evidence for such "camel-shaped" capacitance of electrolytically gated graphene is still missing, the data reported in Ref. [50] do show some asymmetrically positioned, broad peaks in the total capacitance at relatively large applied potentials.

4. Concluding Remarks

We have performed an analysis of the role of dielectric decrement in combination with finite ion size effects for differential capacitance of electrolytically gated graphene using a mean-field theory based variational approach. Extensive comparisons were made with a model combining the finite ion size effects with dielectric saturation in the solvent. Most of our analysis is aided by the fact that expressions for the capacitance are obtained in analytic form, expressing various modifications of the Poisson-Boltzmann theory.

We have started with a thorough discussion of the above models for differential capacitance of a diffuse layer in an aqueous solutions using realistic estimates for various parameters in a broad range of ion concentrations. In particular, we have presented generalizations of the condition for cross-over from a "camel-shaped" to a "bell-shaped" diffuse layer capacitance, taking into account the effects of dielectric decrement and dielectric saturation, in addition to finite ion size effects.

Using a series connection of the quantum capacitance in graphene electrode and the diffuse layer capacitance in the electrolyte, we have confirmed that the total capacitance is dominated by graphene's quantum capacitance at the values of the applied potential $\lesssim 1$ V. At higher potential values, a peak develops in the total capacitance, which can be quite sensitive to the adopted value for the ion size in the presence of dielectric saturation. On the other hand, combining

the finite ion size effect with dielectric decrement yields a rather stable, broad peak in the total capacitance of electrolytically gated graphene at the applied potential values $\gtrsim 1$ V, which persists even in the limit of point ions.

The above discussion is important for future studies of modeling electrolytically gated graphene because typically quite large surface charge densities can be achieved in doped graphene, which may cause extensive ion crowding and high electric fields near graphene that may require taking into account the effects of dielectric decrement and dielectric saturation in the adjacent solution, respectively. The most important next task in those studies should involve realistic modeling of the capacitance for a Stern layer at the graphene-solvent interface. Access to empirical information about the Stern layer capacitance near the potential of zero charge is likely to be severely limited because of the smallness of the quantum capacitance of graphene at small applied potentials. However, regions around possible peaks, or saturation in the total capacitance of electrolytically gated graphene at large applied potentials, could reveal more information regarding the Stern layer at the graphene-solvent interface.

Acknowledgements

This work was supported by the Natural Sciences and Engineering Research Council of Canada (ZLM: grant No. 2016-03689).

References

[1] L. Liu, X. Doug, P. Chen, Critical review: Biological and chemical sensors based on graphene materials, Chem. Soc. Rev. 41 (2012) 2283–2307. doi:10.1039/C1CS15270J.

[2] Y. Yang, A. M. Asiri, Z. Tang, D. Du, Y. Lin, Graphene based materials for biomedical applications, Mater. Today 16 (2013) 365–373. doi:10.1016/j.mattod.2013.09.004.

[3] W. Fu, L. Jiang, E. P. van Geest, L. M. C. Lima, G. F. Schneider, Sensing at the surface of graphene field-effect transistors, Adv. Mater. 29 (2017) 1603610. doi:10.1002/adma.201603610.

[4] L. H. Hess, M. Seifert, J. A. Garrido, Graphene transistors for bioelectronics, Proc. IEEE 101 (2013) 1780–1792. doi:10.1109/JPROC.2013.2261031.

[5] D. J. Cole, P. K. Ang, K. P. Loh, Ion adsorption at the graphene/electrolyte interface, J. Phys. Chem. Lett. 2 (2011) 1799–1803. doi:0.1021/jz200765z.

[6] M. W. Shinwari, M. J. Deen, D. Landheer, Study of the electrolyte-insulator-semiconductor field-effect transistor (eisfet) with applications in biosensor design, Microelectron. Reliab. 47 (2007) 2025–2057. doi:10.1016/j.microrel.2006.10.003.

[7] S. Chen, Z. B. Zhang, L. Ma, P. Ahlberg, Z. Gao, Z. Qiu, D. Wu, W. Ren, H. M. Cheng, S. L. Zhang, A graphene field-effect capacitor sensor in electrolyte, Applied Phys. Lett. 101 (2012) 154106. doi:10.1063/1.4759147.

[8] T. Fang, A. Konar, H. L. Xing, D. Jena, Carrier statistics and quantum capacitance of graphene sheets and ribbons, Appl. Phys. Lett. 91 (2007) 092109. doi:10.1063/1.2776887.

[9] J. Xia, F. Chen, J.Li, N. Tao, Measurement of the quantum capacitance of graphene, Nature Nano. 4 (2009) 505–509. doi:10.1038/nnano.2009.177.

[10] H. Xu, Z. Zhang, L.-M. Peng, Measurements and microscopic model of quantum capacitance in graphene, Appl. Phys. Lett. 98 (2011) 133122. doi:10.1063/1.3574011.

[11] C. H. Kim, C. D. Frisbie, Determination of quantum capacitance and band filling potential in graphene transistors with dual electrochemical and field-effect gates, J. Phys. Chem. C 118 (2014) 21160–21169. doi:10.1021/jp505391u.

[12] I. Heller, S. Chatoor, J. Männik, M. A. G. Zevenbergen, C. Dekker, S. G. Lamay, Influence of electrolyte composition on liquid gated carbon nanotube and graphene transistors, J. Am. Chem. Soc. 132 (2010) 17149–17156. doi:10.1021/ja104850n.

[13] H. Ji, X. Zhao, Z. Qiao, J. Jung, Y. Zhu, Y. Lu, L. L. Zhang, A. H. MacDonald, R. S. Ruoff, Capacitance of carbon-based electrical double-layer capacitors, Nat. Commun. 5 (2014) 3317. doi:10.1038/ncomms4317.

[14] F. Chen, Q. Qing, J. Xia, N. Tao, Graphene field-effect transistors: Electrochemical gating, interfacial capacitance, and biosensing applications, Chem. Asian J. 5 (2010) 2144–2153. doi:10.1002/asia.201000252.

[15] G. Jiang, C. Cheng, D. Li, J. Z. Liu, Molecular dynamics simulations of the electric double layer capacitance of graphene electrodes in mono-valent aqueous electrolytes, Nano Research 9 (2016) 174–186. doi:10.1007/s12274-015-0978-5.

[16] I. C. Yeh, M. L. Berkowitz, Dielectric constant of water at high electric fields: Molecular dynamics studies, J. Chem. Phys. 110 (1999) 7935–7942. doi:10.1063/1.478698.

[17] L. Sandberg, R. Edholm, Nonlinear response effects in continuum models of the hydration of ions, J. Chem. Phys. 116 (2002) 2936–2944. doi:10.1063/1.1435566.

[18] R. L. Fulton, The nonlinear dielectric behavior of water: Comparisons of various approaches to the nonlinear dielectric increment, J. Chem. Phys. 130 (2009) 204503. doi:10.1063/1.313921.

[19] M. Aguilella-Arzo, A. Andrio, V. M. Aguilella, A. Alcaraz, Dielectric saturation of water in a membrane protein channel, Phys. Chem. Chem. Phys. 11 (2009) 358–365. doi:10.1039/B812775A.

[20] L. Pilon, H. Wang, A. d'Entremont, Recent advances in continuum modeling of interfacial and transport phenomena in electric dou-

ble layer capacitors, J. Electrochem. Soc. 162 (2015) A5158–A5178. doi:10.1149/2.0211505jes.

[21] I. Borukhov, D. Andelman, H. Orland, Steric effects in electrolytes: A modified poisson-boltzmann equation, Phys. Rev. Lett. 79 (1997) 435–438. doi:10.1103/PhysRevLett.79.435.

[22] M. S. Kilic, M. Z. Bazant, A. Ajdari, Steric effects in the dynamics of electrolytes at large applied voltages. i. double-layer charging, Phys. Rev. E 75 (2007) 021502. doi:10.1103/PhysRevE.75.021502.

[23] A. A. Kornyshev, Double-layer in ionic liquids: paradigm change?, J. Phys. Chem. B 111 (2007) 5545–5557. doi:10.1021/jp067857o.

[24] M. Z. Bazant, M. S. Kilic, B. D. Storey, A. Ajdari, Towards an understanding of induced-charge electrokinetics at large applied voltages in concentrated solutions, Adv. Colloid Interface Sci. 152 (2009) 48–88. doi:10.1016/j.cis.2009.10.001.

[25] D. Ben-Yaakov, D. Andelman, D. Harries, R. Podgornik, Beyond standard poisson-boltzmann theory: Ion-specific interactions in aqueous solutions, J. Phys.: Condens. Matter 21 (2009) 424106. doi:10.1088/0953-8984/21/42/424106.

[26] P. Sharma, Z. L. Miskovic, Capacitance of graphene in aqueous electrolytes: The effects of dielectric saturation of water and finite size of ions, Phys. Rev. B 90 (2014) 125415. doi:10.1103/PhysRevB.90.125415.

[27] L. Daniels, M. Scott, Z. L. Mišković, The role of stern layer in the interplay of dielectric saturation and ion steric effects for the capacitance of graphene in aqueous electrolytes, J. Chem. Phys. 146 (2017) 094101. doi:10.1063/1.4976991.

[28] J. J. Bikerman, Structure and capacity of the electrical double layer, Philos. Mag. 33 (1942) 384–397. doi:0.1080/14786444208520813.

[29] V. Freise, Zur theorie der diffusen doppelschicht, Z. Elektrochem. 56 (1952) 822–827. doi:10.1002/bbpc.19520560826.

[30] F. Booth, The dielectric constant of water and the saturation effect, J. Chem. Phys. 19 (1951) 391–394. doi:10.1063/1.1748233.

[31] D. Ben-Yaakov, D. Andelman, R. Podgornik, Dielectric decrement as a source of ion-specific effects, J. Chem. Phys. 134 (2011) 074705. doi:10.1063/1.3549915.

[32] M. M. Hatlo, R. van Roij, L. Lue, The electric double layer at high surface potentials: The influence of excess ion polarizability, EPL 97 (2012) 28010. doi:10.1209/0295-5075/97/28010.

[33] Y. Nakayama, D. Andelman, Differential capacitance of the electric double layer: The interplay between ion finite size and dielectric decrement, J. Chem. Phys. 142 (2015) 044706. doi:10.1063/1.4906319.

[34] G. Minton, L. Lue, The influence of excluded volume and excess ion polarisability on the capacitance of the electric double layer, Mol. Phys. 114 (2016) 2477–2491. doi:10.1080/00268976.2016.1169327.

[35] N. Gavish, K. Promislow, Dependence of the dielectric constant of electrolyte solutions on ionic concentration: A microfield approach, Phys. Rev. E 94 (2016) 012611. doi:10.1103/PhysRevE.94.012611.

[36] B. Figliuzzi, W. H. R. Chan, C. R. Buie, J. L. Moran, Nonlinear electrophoresis in the presence of dielectric decrement, Phys. Rev. E 94 (2016) 023115. doi:10.1103/PhysRevE.94.023115.

[37] J. López-García, J. Horno, C. Grosse, Differential capacitance of the diffuse double layer at electrode-electrolyte interfaces considering ions as dielectric spheres: Part 1. binary electrolyte solutions, J. Coll. and Inter. Sci. 496 (2017) 531–539. doi:10.1016/j.jcis.2017.02.043.

[38] J. B. Hasted, D. M. Ritson, C. H. Collie, Dielectric properties of aqueous ionic solutions. parts i and ii, J. Chem. Phys. 16 (1948) 1–21. doi:10.1063/1.1746645.

[39] M. V. Fedorov, A. A. Kornyshev, Ionic liquids at electrified interfaces, Chem Rev. 114 (2014) 2978–3036. doi:10.1021/cr400374x.

[40] Z. A. H. Goodwin, G. Feng, A. A. Kornyshev, Mean-field theory of electrical double layer in ionic liquids with account of short-range correlations, Electrochim. Acta 225 (2017) 190–197. doi:10.1016/j.electacta.2016.12.092.

[41] J.-P. Randin, E. Yeager, Differential capacitance study of stress-annealed pyrolytic graphite electrodes, J. Electrochem. Soc. 118 (1971) 711–714. doi:10.1149/1.2408151.

[42] J.-P. Randin, E. Yeager, Differential capacitance study on basal plane of stress-annealed pyrolytic-graphite, J. Electroanal. Chem. 36 (1972) 257–276. doi:10.1016/S0022-0728(72)80249-3.

[43] H. Gerischer, An interpretation of the double layer capacity of graphite electrodes in relation to the density of states at the fermi level, J. Phys. Chem. 89 (1985) 4249–4251. doi:10.1021/j100266a020.

[44] M. Hahn, M. Baertschi, O. Barbieri, J.-C. Sauter, R. Kotz, R. Gallay, Interfacial capacitance and electronic conductance of activated carbon double-layer electrodes, Electrochem. Solid-State Lett. 7 (2004) A33–A36. doi:10.1149/1.1635671.

[45] A. A. Kornyshev, N. B. Luque, W. Schmickler, Differential capacitance of ionic liquid interface with graphite: the story of two double layers, J. Solid State Electrochem. 18 (2014) 1345–1349. doi:10.1007/s10008-013-2316-8.

[46] A. A. Kornyshev, E. Spohr, M. A. Vorotyntsev, Electrochemical Interfaces: At the Border Line, Wiley, New York, 2002, Ch. 2, pp. 33–132. doi:10.1002/9783527610426.bard010201.

[47] A. A. Kornyshev, M. A. Vorotyntsev, Nonlocal dielectric response of the electrode/solvent interface in the double layer problem, Canad. J. Chem. 59 (1981) 2031–2042. doi:10.1139/v81-299.

[48] A. A. Kornyshev, W. Schmickler, M. A. Vorotyntsev, Nonlocal electrostatic approach to the problem of a double layer at a metal-electrolyte interface, Phys. Rev. B 25 (1982) 5244–5256. doi:10.1103/PhysRevB.25.5244.

[49] M. V. Fedorov, A. A. Kornyshev, Towards understanding the structure and capacitance of electrical double layer in ionic liquids, Electrochim. Acta 53 (2008) 6835–6840. doi:10.1016/j.electacta.2008.02.065.

[50] X. Du, H. Guo, Y. Jin, Q. Jin, J. Zhao, Electrochemistry investigation on the graphene/electrolyte interface, Electroanalysis 27 (2015) 2760–2765. doi:10.1002/elan.201500302.

Highlights

- First study of dielectric decrement and steric effects for graphene in electrolyte
- New condition for crossover from camel- to bell-shaped diffuse layer capacitance
- Novel analytical treatment of diffuse layer capacitance based on Eq.(8)
- Comparisons with analogous effects for dielectric saturation and steric effects
- All 3 effects are important due to large charge density on graphene in experiments

Graphical Abstract